

# Supplementary Information

## Plasmonic Hot Carrier Injection from Single Gold Nanoparticles into Topological Insulator Bi<sub>2</sub>Se<sub>3</sub> Nanoribbons.

Christian Nweze,<sup>\*a</sup> Tomke E. Glier,<sup>a</sup> Mika Rerrer,<sup>a</sup> Sarah Scheitz,<sup>a</sup> Yalan Huang,<sup>b</sup> Robert Zierold,<sup>b</sup> Robert Blick,<sup>b</sup> Wolfgang J. Parak,<sup>b</sup> Nils Huse,<sup>b</sup> and Michael Rübhausen<sup>\*a</sup>

<sup>a</sup>Institut für Nanostruktur- und Festkörperphysik, Center for Free Electron Laser Science (CFEL), Universität Hamburg, Luruper Chaussee 149, 22761, Hamburg, Germany

<sup>b</sup>Institut für Nanostruktur- und Festkörperphysik, Center for Hybrid Nanostructures (CHyN), Universität Hamburg, Luruper Chaussee 149, Hamburg, 22761 Germany

### A. Experimental procedure

Single crystalline Bi<sub>2</sub>Se<sub>3</sub> nanoribbons were grown in a two-heating zone furnace in a chemical vapor deposition (CVD) set up. The furnace was equipped with a quartz tube of diameter 2.5 cm. The Bi<sub>2</sub>Se<sub>3</sub> nanoribbons were grown on silicon ⟨100⟩ substrates with native oxide (SiO<sub>2</sub>) layer. We followed a general approach in CVD method [1]–[3] with full optimization for growth of Bi<sub>2</sub>Se<sub>3</sub> nanoribbons. The growth process involves: (a) cleaning the 1x1 cm silicon ⟨100⟩ substrates in Piranha solution and rinsing in deionized water in order to remove dirt, (b) functionalizing the substrates with 0.1% w/v aqueous poly-L-lysine to enhance gold attachment to the substrates, (c) dipping the substrates in colloid solution of gold (50 nm diameter) for 5 s, and (d) growth of Bi<sub>2</sub>Se<sub>3</sub> nanoribbons on the functionalized substrates. The source material is a commercial grade Bi<sub>2</sub>Se<sub>3</sub> granular (Sigma-Aldrich, purity 99.999%). 0.2 g of granular Bi<sub>2</sub>Se<sub>3</sub> was used for the synthesis. The granular Bi<sub>2</sub>Se<sub>3</sub> was placed in an alumina boat and loaded at the upstream zone of the furnace and the gold coated 1x1 cm silicon substrates were loaded at the downstream zone of the furnace. The tube was pumped to a pressure of 40 mTorr, and flushed multiple times with ultrapure argon gas to minimize oxygen contamination in the quartz tube. For synthesis, the downstream and upstream zones were heated in 1 hour from room temperature to 440 °C and 540 °C respectively. The carrier gas flow rate and the pressure were set to 30 standard cubic centimeters per minute and 780 mTorr, respectively. The reaction time was 1 hour. In order to provide a selenium environment and to

protect the surface of  $\text{Bi}_2\text{Se}_3$  with selenium powder, after the reaction, the argon flow was switched off and the system was allowed to cool down to room temperature in 2.5 h. To validate the quality of the grown samples, various characterization techniques were employed. A custom-made x, y, z – positioner micro-manipulator was used to transfer the nanoribbons to a custom-made silicon finder grid with 225 fields of  $100\ \mu\text{m} \times 100\ \mu\text{m}$ . The positioner has 51 mm long tungsten picoprobe tips (T-4-10) with a wire shaft diameter of  $10\ \mu\text{m}$ , a point radius  $< 0.1\ \mu\text{m}$ , and a tip length of 3.3 mm. The atomic force microscopy (AFM, Q-Scope 250 model with  $40\ \mu\text{m} \times 40\ \mu\text{m}$  scan head with a lateral and vertical resolutions of 0.6 nm and 0.05 nm, respectively) was used to determine the thickness (height) of the nanoribbons. Scanning electron microscope (SEM, ZEISS SIGMA) was used to determine the width of the nanoribbons. Energy dispersive x-ray spectroscopy (EDX, ZEISS) was used to determine the stoichiometry of the nanoribbons.

## **B. Synthesis and characterization of gold nanoparticles**

The synthesis of the spherical citrate-stabilized gold nanoparticles (AuNPs) of different sizes was prepared as previously reported [4]. According to the chosen growth speed of the AuNPs in our method, the mean core size  $d_{c, TEM}$  of the AuNPs was expected to be around 100 nm. The AuNPs used in this manuscript were double phase-transferred and finally coated with PMA-g-dodecyl, an amphiphilic polymer which is based on a backbone of poly(isobutylene-alt-maleic anhydride), functionalized with dodecylamine [4].

The UV/vis absorption spectra of the PMA-g-dodecyl coated AuNPs as dispersed in water was recorded with an Agilent 8453 spectrophotometer as previously reported [4]. NPs were dispersed in water, see Fig. S1(a). The wavelength of the surface plasmon peak was  $\lambda_{SPR} = 578\ \text{nm}$  (table S1)

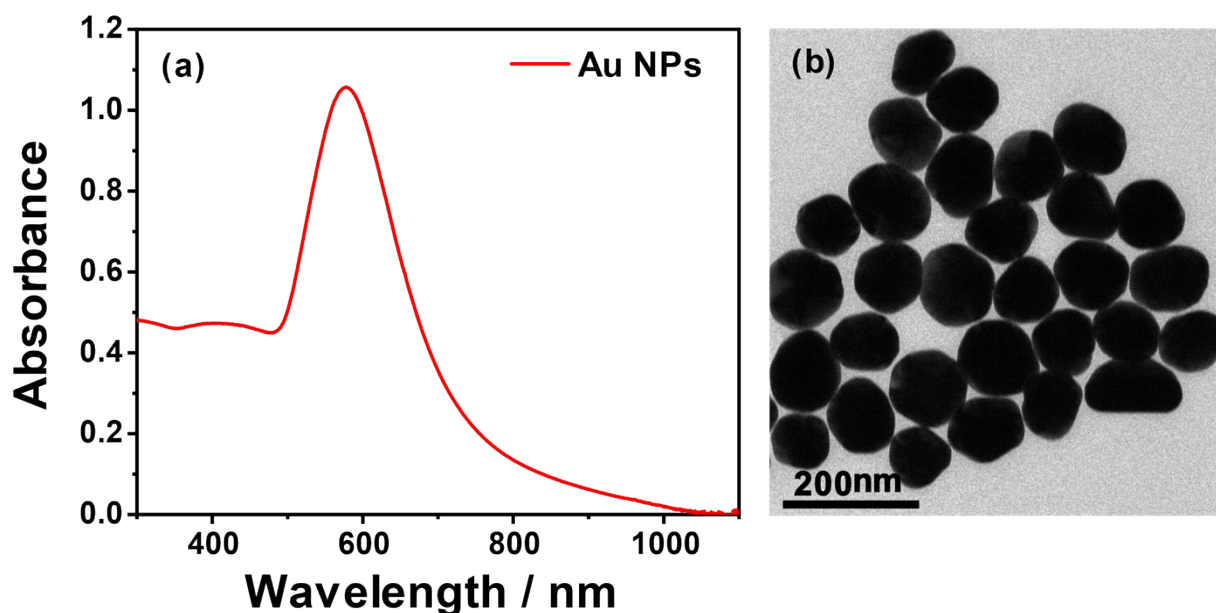


Figure S1. (a) UV/vis absorbance spectrum of the AuNPs. (b) Representative TEM image of the AuNPs.

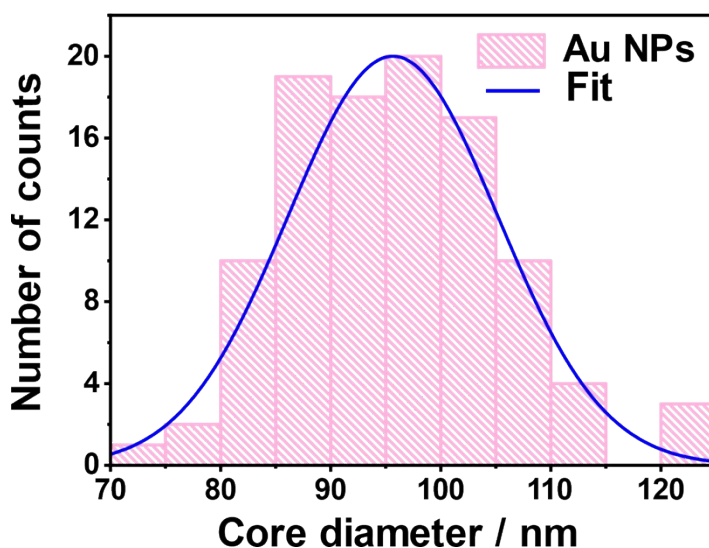


Figure S2. Histogram of the core diameter distribution  $N(d_{c,TEM})$  as determined from the TEM images, and a corresponding Gaussian fit. The mean value of  $d_{c,TEM}$  as displayed in Table S1 was calculated from 100 AuNPs.

Transmission electron microscopy (TEM) images were used to investigate the size distribution of the AuNP diameter. In order to determine the size distribution of the core diameter  $d_{c,TEM}$  of the AuNPs,  $d_{c,TEM}$  was determined as mean value from 100 NPs in the TEM images using the ImageJ software [4]. Illustrative TEM images of the AuNPs are displayed in Fig. S1(b) and the obtained size distribution histograms and further characterization can be seen in Fig. S2 and table S1.

**Table S1.** Characterization table of the AuNPs

$\lambda_{\text{SPR}} / \text{nm}$	$d_{\text{c,TEM}} / \text{nm}$	$d_{\text{h(N)}} / \text{nm}$	$d_{\text{h(V)}} / \text{nm}$	$d_{\text{h(I)}} / \text{nm}$	$\zeta / \text{mV}$
578	95.7 $\pm$ 9.6	76.9 $\pm$ 3.7	127.5 $\pm$ 3.4	130.3 $\pm$ 2.7	-39.0 $\pm$ 0.4

In order to determine the hydrodynamic diameters  $d_h$  of the AuNPs as dispersed in water, dynamic light scattering (DLS) was used [4]. Also, the zeta potential  $\zeta$  of the AuNP solution was measured with laser Doppler anemometry (LDA). DLS and LDA were carried out using a Malvern Zetasizer ZS instrument. Data are presented in Fig. S3 and table S1.

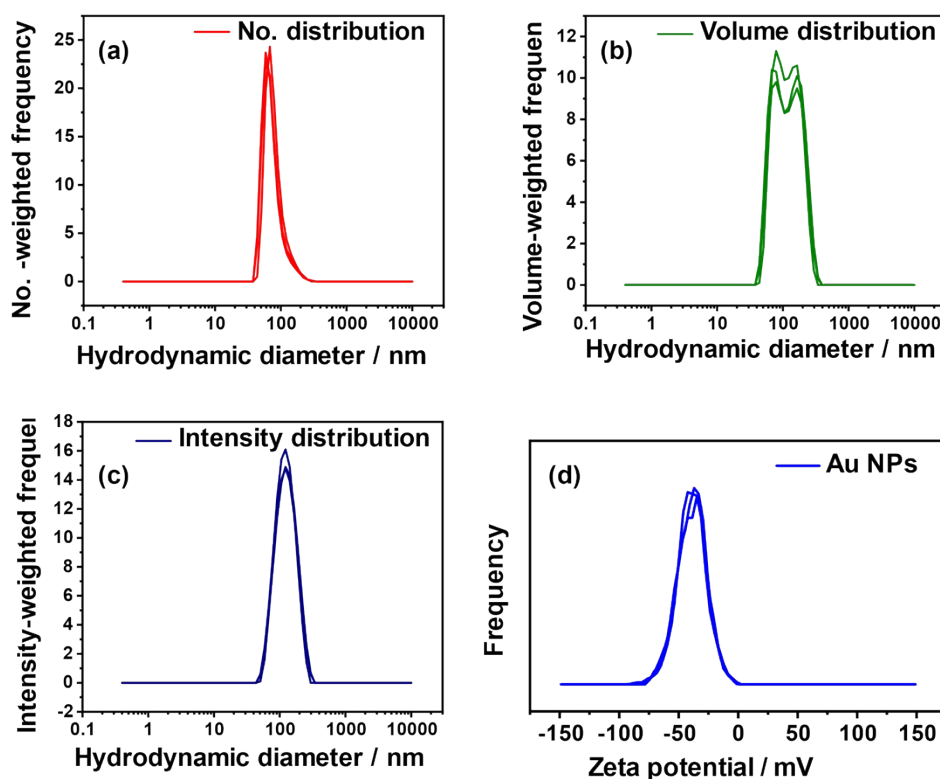


**Figure S3.** Distribution the hydrodynamic diameter  $d_h$  of the AuNPs recorded by DLS based on (a) the number distribution  $N^{(d_{h(N)})}$ , (b) the volume distribution  $N^{(d_{h(V)})}$ , and (c) the intensity distribution  $N^{(d_{h(I)})}$ . (d) Zeta potential of the AuNPs. The obtained mean values for the hydrodynamic diameters and zeta potential are shown in Table S1.

### C. Decorating the $\text{Bi}_2\text{Se}_3$ nanoribbons with gold nanoparticles

$10 \mu\text{L}$  of the dispersed AuNPs in water was drop cast on the  $\text{Bi}_2\text{Se}_3$  nanoribbons and dried before characterization.

### D. Characterization

$\text{Bi}_2\text{Se}_3$  nanoribbons were characterized before the Raman study. The width of the nanoribbons was measured via AFM and SEM. The exemplary SEM images for the  $\text{Bi}_2\text{Se}_3$  nanoribbons of width 210 nm and 292 nm (thickness 100 nm and 90.1 nm) are shown in Figs. S4 (b and c), respectively. The quantitative analysis of the SEM-EDX data collected from the nanoribbons shows the correct stoichiometry (2:3 (Bi:Se)) as shown in Fig. S4 (a). The silicon peak in the spectra comes from the silicon substrate. The thickness of the  $\text{Bi}_2\text{Se}_3$  nanoribbons was obtained with an AFM. Figs. S5 (a - d) show exemplary AFM images of the  $\text{Bi}_2\text{Se}_3$  nanoribbons of thickness 47 nm and 90 nm.

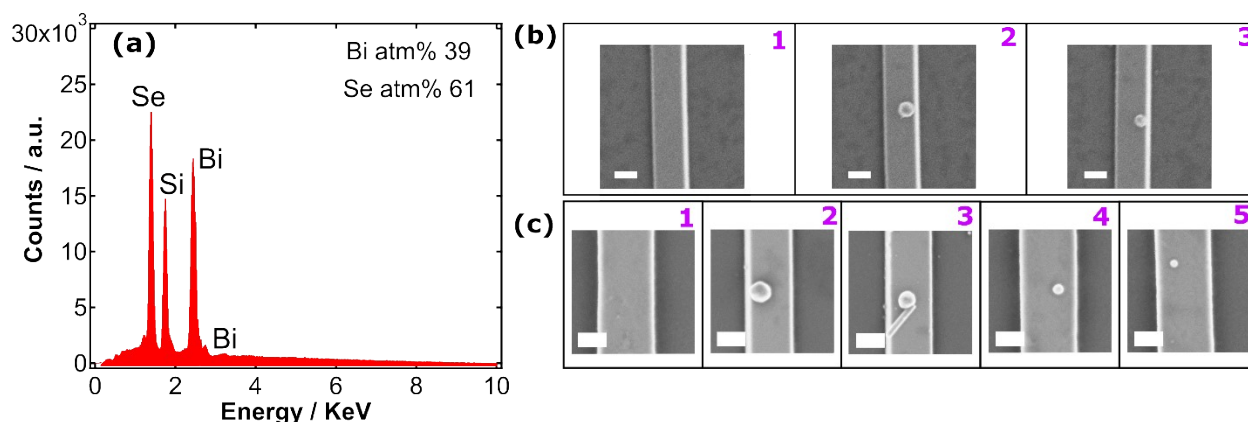


**Figure S4.** (a) EDX spectra acquired from  $\text{Bi}_2\text{Se}_3$  nanoribbons. Quantitative analysis of the EDX data shows a composition of 39 atm% Bi and 61 atm% Se. The silicon peak comes from the silicon substrate. Exemplary SEM images of  $\text{Bi}_2\text{Se}_3$  nanoribbons with (b) width of 210 nm and thickness of 100 nm, (c) width of 292 nm and thickness of 90.1 nm are shown. The  $\text{Bi}_2\text{Se}_3$  nanoribbons have single AuNP of different sizes. The scale bar represents a length of 200 nm.

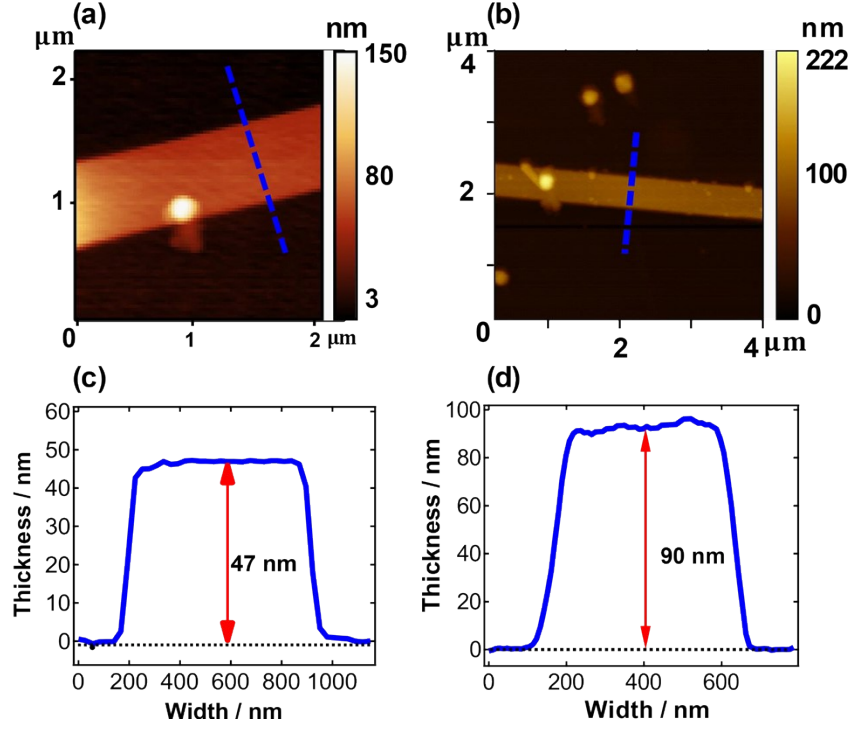


**Figure S5.** Exemplary AFM images and height profiles. The height of (c)  $47 \pm 1$  nm, and (d)  $90 \pm 2$  nm was obtained from the AFM images (a) and (b), respectively. Blue dotted lines indicate the location of the height profiles.

### E. Crystal structure, Raman tensors and atomic displacements of $\text{Bi}_2\text{Se}_3$

The crystal structure, Raman tensors and atomic displacements of the Raman active modes in  $\text{Bi}_2\text{Se}_3$  are shown in Fig. S6. The Raman tensors show that the  $E_g$  – mode has non-vanishing off-diagonal elements in comparison with the vanishing components in the off-diagonal elements of  $A_{1g}$  – mode [5].

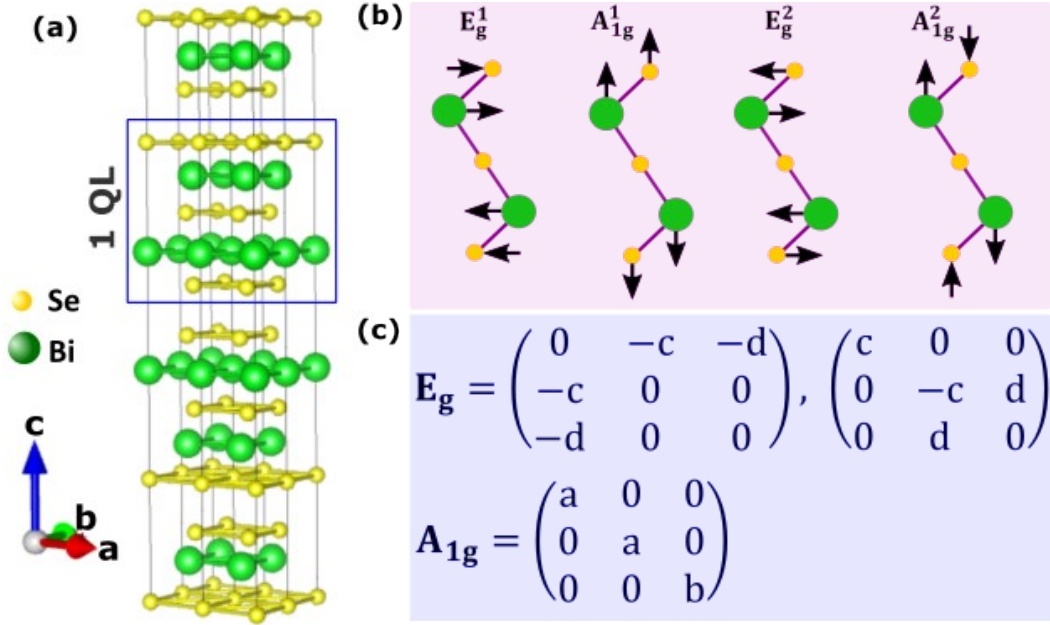


**Figure S6.** (a) Crystal structure showing quintuple layer, (b) atomic displacement of Raman active modes showing in and out of plane vibrations and (c) Raman tensors of  $\text{Bi}_2\text{Se}_3$ .

## F. Raman study

The  $\text{Bi}_2\text{Se}_3$  nanoribbons were pre-characterized before Raman study. Raman spectroscopy of Au decorated single nanoribbons was carried out at room temperature with a custom-made micro-Raman set-up [6], [7]. With the aid of a 50x objective (Plan Apo HR, Mitutoyo, Japan), with numerical aperture (NA) of 0.75, the backscattered Raman signal was collected and focused into the entrance objective of the fully reflective UT-3 spectrometer [6]. The beam spot size of the micro-Raman is between  $211 \pm 3 - 389 \pm 3$  nm depending on the excitation wavelength. For a 633 nm wavelength, the full width at half maximum (FWHM) is  $211 \pm 3$  nm. Fig. S7 shows an exemplary image of a 633 nm laser spot focused on silicon substrate and the intensity cuts in four different directions through the laser spot. The intensity is fitted with a Gaussian profile. The measurement was done in back-scattering configuration while employing Porto notation  $\bar{Z}(XX)Z$  configuration [8] (Fig. S8(b)). The spectra were acquired in 20 mins. In order to exclude laser heating of the samples, the laser power on the sample surface is kept less than  $50 \mu\text{W}$ . Several pre-test measurements were carried out on different  $\text{Bi}_2\text{Se}_3$  nanoribbons before the actual

measurement. The laser sources used for the resonance study were (a) red laser, 633 nm wavelength (Gas, 05-LHP-123-496 HeNe), (b) yellow laser, 594 nm wavelength (Diode, OBIS 594LS 1233468), (c) greenish-yellow laser, 560 nm wavelength (Diode, OBIS 561LS 1223779) and (d) green laser, 532 nm wavelength (Diode, Millenia Pro 10sJS). Note that the pre-test measurement was done on the  $\text{Bi}_2\text{Se}_3$  nanoribbons from the same synthesis used in this study.

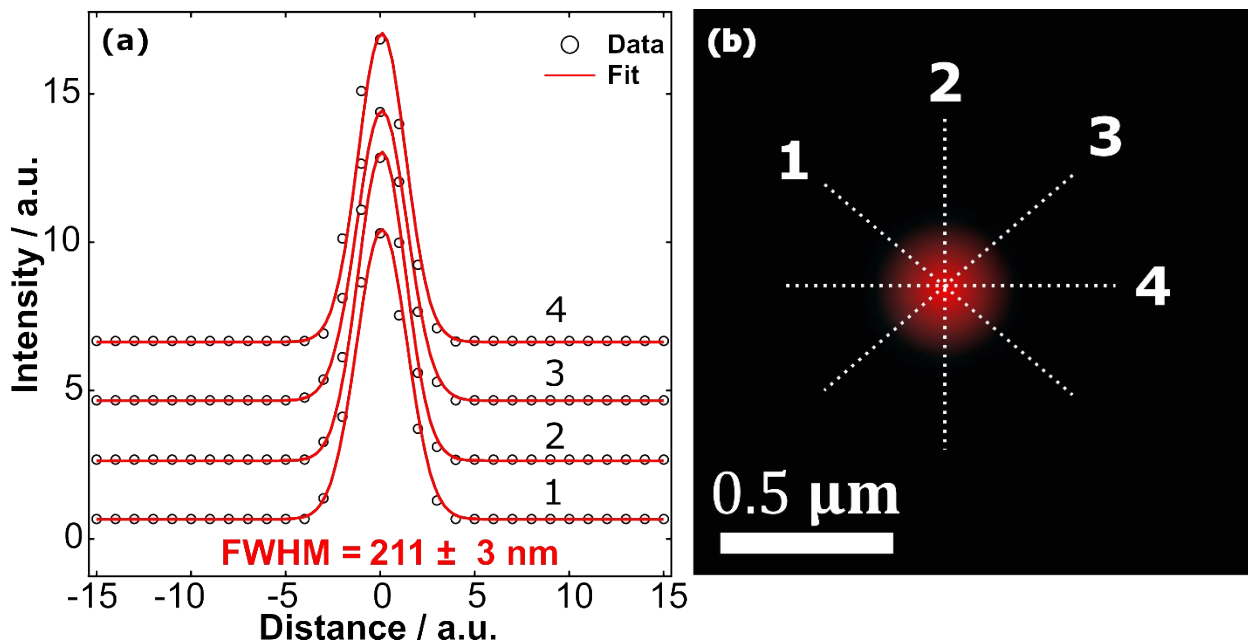


**Figure S7.** Exemplary red laser beam spot diameter. (a) The intensity profile for four different directions (1-4) fitted with a Gaussian profile. The resulting FWHM has an average value of  $211 \pm 3$  nm. (b) 2D image of red laser spot showing intensity cuts in four different directions.

## G. Polarization dependence study

We conducted a polarization dependence study on our sample. The angle between the incident and scattered polarized light is tuned from  $0^\circ - 90^\circ$ . For  $\bar{Z}(XX)Z$ , the angle is  $0^\circ$  and it corresponds to the x-x component of the Raman tensors (Fig. S8 (b)). For  $\bar{Z}(YX)Z$ , the angle is  $90^\circ$  and it corresponds to the y-x component of the Raman tensors (Fig. S8 (c)). Fig. S5(a) shows the Raman spectra of  $\text{Bi}_2\text{Se}_3$  for On\_AuNP (blue) and Off\_AuNP (red) positions. The result shows that the intensities of  $A_{1g}^1$  and  $A_{1g}^2$  – modes have reduced considerably for the perpendicular polarized state in comparison to the parallel polarized state. Furthermore, the intensity of the  $E_g^2$  remains unaltered in adherence to the Raman tensor of Fig. S6(c). This dependence of  $A_{1g}^1$  and  $A_{1g}^2$  – modes on polarization indicates that our  $\text{Bi}_2\text{Se}_3$  sample is single crystalline [9]. Note that the sensitivity of the UT-3 spectrometer at 633 nm wavelength is 41% and 4% for horizontal (parallel) and vertical (perpendicular) polarized light, respectively [6].

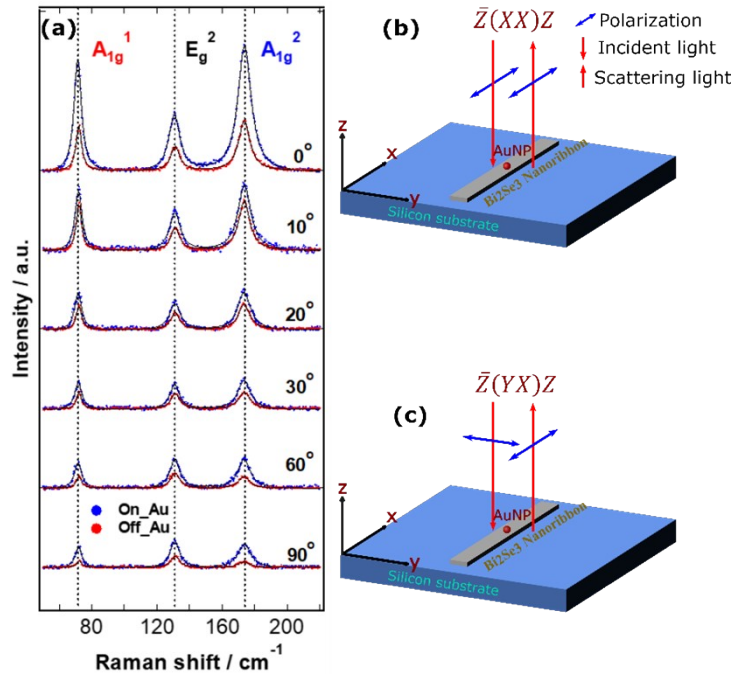


**Figure S8.** Polarization dependence Raman studies of  $\text{Bi}_2\text{Se}_3$  nanoribbon with a thickness of 83 nm and width of 300 nm and decorated with a single AuNP of diameter 128 nm. (a) Raman spectra of  $\text{Bi}_2\text{Se}_3$  nanoribbon at different polarized angles. The spectra acquired in On\_AuNP and Off\_AuNP positions are represented in blue and red colours, respectively. The parallel and perpendicular polarization of the incident and scattered lights are shown in (b) and (c), respectively.

## H. Ratio between the FWHM of $A_{1g}^2/A_{1g}^1$ and $E_g^2/A_{1g}^1$ modes

The ratio between the FWHM of  $A_{1g}^2/A_{1g}^1$  (blue symbol) and  $E_g^2/A_{1g}^1$  (black symbol) as a function of distance from the AuNP (Fig. S9). The solid blue and black lines are the Gaussian fit to the data. The broadening of the phonon modes at On\_Au position shows strong electron-phonon interaction as a result of high density of hot injected electrons around the AuNP. The density of these hot electrons decreases with distance from AuNP along the nanoribbon and hence, the electron phonon interaction weakens on scanning away from the AuNP.

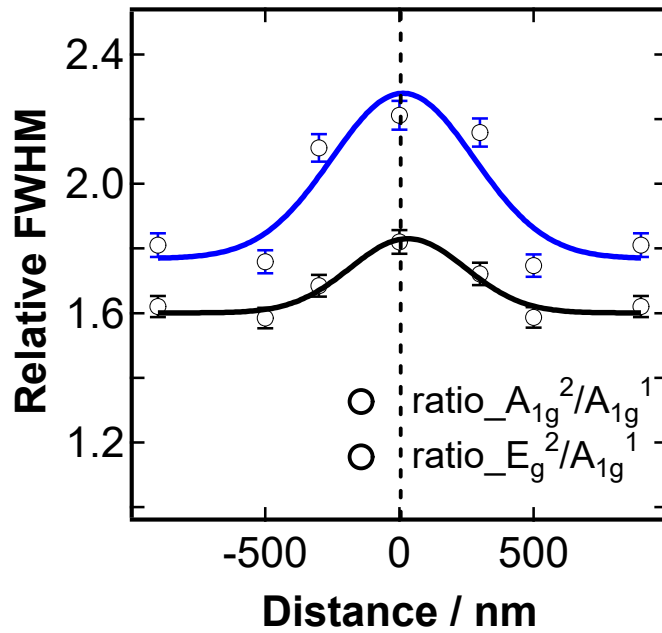


**Figure S9.** Plot of the relative FWHM as a function of distance from the AuNP. The blue and black symbols represent the ratio of  $A_{1g}^2/A_{1g}^1$  and  $E_g^2/A_{1g}^1$ , respectively. The solid lines represent the Gaussian fit to the data.

## I. Contribution from AuNP itself and from injected hot carrier

In order to discriminate the contribution from AuNP and from the injected carriers, we conducted further studies (reference measurement) on silicon substrate decorated with 120, 107 and 104 nm AuNPs (Fig. S10). We observe an enhancement factor of 1.043 which is drastically different compared to what we see in topological insulators.

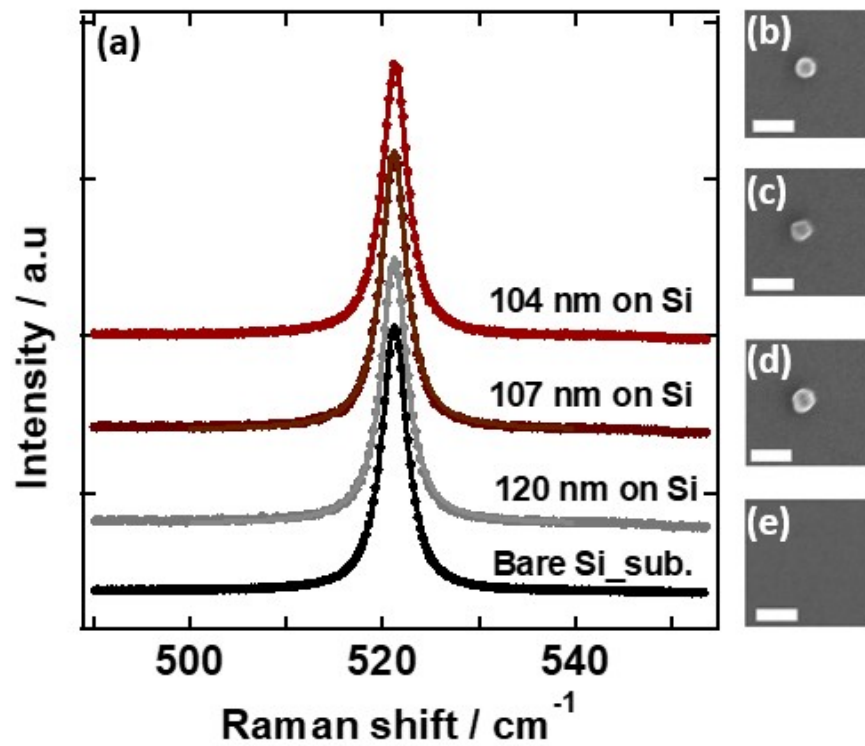


**Figure S10.** Raman studies on silicon substrate (of 100 nm native oxide layer) decorated with (b) 104, (c) 107, (d) 120 nm AuNPs, and (e) bare silicon substrate as shown in the label. Each scale bar represents a length of 200 nm. (a) Raman spectra of silicon substrate decorated with AuNPs. The spectra were vertically shifted for clarity and fitted with Lorentzian profiles.

## References

- [1] H. Peng *et al.*, "Aharonov-Bohm interference in topological insulator nanoribbons," *Nature Materials*, vol. 9, no. 3, pp. 225–229, 2010, doi: 10.1038/nmat2609.
- [2] D. Kong *et al.*, "Topological insulator nanowires and nanoribbons," *Nano Letters*, vol. 10, no. 1, pp. 329–333, Jan. 2010, doi: 10.1021/nl903663a.
- [3] Y. Yan *et al.*, "Synthesis and quantum transport properties of Bi<sub>2</sub>Se<sub>3</sub> topological insulator nanostructures," *Scientific Reports*, vol. 3, 2013, doi: 10.1038/srep01264.
- [4] J. Hühn *et al.*, "Selected standard protocols for the synthesis, phase transfer, and characterization of inorganic colloidal nanoparticles," *Chemistry of Materials*, vol. 29, no. 1, pp. 399–461, Jan. 2017, doi: 10.1021/acs.chemmater.6b04738.
- [5] W. Richter, H. Koi-Iler, and C. R. Becker, "A Raman and Far-Infrared Investigation of Phonons in the Rhombohedra1 V2-V13 Compounds Bi<sub>2</sub>Te<sub>3</sub>, Bi<sub>2</sub>Se<sub>3</sub>, Sb<sub>2</sub>Te<sub>3</sub> and Bi<sub>2</sub>(Te<sub>14</sub>Se<sub>3</sub>)<sub>3</sub> (0 < x < 1), (Bi<sub>1</sub>Sb<sub>y</sub>)<sub>2</sub>Te<sub>3</sub> (0 < y < 1)."
- [6] B. Schulz *et al.*, "Fully reflective deep ultraviolet to near infrared spectrometer and entrance optics for resonance Raman spectroscopy," *Review of Scientific Instruments*, vol. 76, no. 7, Jul. 2005, doi: 10.1063/1.1946985.
- [7] T. E. Glier, "Applications of Functional One-Dimensional Nanostructures Studied by Light Scattering," University of Hamburg, 2021.
- [8] T. C. Damen, S. P. Porto, and B. TELL, "Raman Effect in Zinc Oxide," Academic Press Inc, 1966.
- [9] B. Irfan *et al.*, "Temperature dependent Raman scattering studies of three dimensional topological insulators Bi<sub>2</sub>Se<sub>3</sub>," in *Journal of Applied Physics*, May 2014, vol. 115, no. 17. doi: 10.1063/1.4871860.